

Photo-realistic Image Super-resolution with Fast and Lightweight Cascading Residual Network

Namhyuk Ahn, Byungkon Kang, and Kyung-Ah Sohn

Abstract—Recent progress in the deep learning-based models has improved single-image super-resolution significantly. However, despite their powerful performance, many models are difficult to apply to the real-world applications because of the heavy computational requirements. To facilitate the use of a deep learning model in such demands, we focus on keeping the model fast and lightweight while maintaining its accuracy. In detail, we design an architecture that implements a cascading mechanism on a residual network to boost the performance with limited resources via multi-level feature fusion. Moreover, we adopt group convolution and weight-tying for our proposed model in order to achieve extreme efficiency. In addition to the traditional super-resolution task, we apply our methods to the photo-realistic super-resolution field using the adversarial learning paradigm and a multi-scale discriminator approach. By doing so, we show that the performances of the proposed models surpass those of the recent methods, which have a complexity similar to ours, for both traditional pixel-based and perception-based tasks.

Index Terms—Super-resolution, Photo-realistic, Deep Learning, Convolutional Neural Network, Efficient Model

I. INTRODUCTION

Image super-resolution (SR) is a longstanding computer vision task that can be widely used in numerous applications. It focuses on recovering a high-resolution (HR) image from low-resolution (LR) images. In particular, single-image super-resolution (SISR) performs SR using a single LR image. Since the SISR problem is a many-to-one mapping, constructing an effective SISR algorithm is a challenging task. In spite of the difficulties, SISR has been actively studied because it can potentially be applied to a variety of services. In recent, deep learning-based methods have shown prominent performance on SISR task [1]–[3]. The major trend of these algorithms is stacking more layers to their models to achieve a more accurate result. For instance, SRCNN [1], the first model applying deep learning, has only three convolutional layers, but the recent model RCAN [4] has 400 layers. However, while deep learning-based algorithms increase the quality of the SR images significantly, using these models for the real-world scenarios is another challenge. There are many cases that require not only the performance but also efficiency, such as streaming services or mobile platform-based applications. From this point of view, it is important to design a lightweight model that is practical for such demands.

One way to build a lean model is to reduce the number of parameters. There are many ways to achieve this [5], [6]. One of the most simple and effective approach is to construct the network in a recursive manner. However, even though models with recursive structures [7], [8] show good performance and efficiency in terms of the parameters, they have two downsides:

- 1) They first upsample the input image before feeding it to the CNN model, and
- 2) they increase the depth or the width of the network to compensate for the performance loss caused by the use of a recursive network. These characteristics enable the model to maintain the details of the images when reconstructed, but at the expense of the increased number of operations and inference time.

Excluding the aforementioned methods, much of the work that aims to build a lean model has focused primarily on reducing the number of parameters. However, as mentioned earlier, the number of operations is also an important factor to consider in real-world demands. For the SR systems that operate on mobile devices, the execution speed also plays an important role from a user-experience perspective. Especially the battery capacity, which is heavily dependent on the amount of computation performed, becomes a major problem. In this respect, reducing the number of operations is a challenging and necessary step that has largely been ignored until now. Another scenario relates to applying SR methods to video streaming services. The demand for streaming media has skyrocketed and hence requires large storage for massive multimedia data. It is therefore imperative to compress data using lossy compression techniques before storing. Then, an SR technique can be applied to restore the data to the original resolution. However, because latency is the most critical factor in such services, the decompression process has to be performed close to real-time. To do so, it is essential to make the SR methods lightweight in terms of the number of operations.

Along with the above requirement, we also focus on solving photo-realistic SR. This task recently gained attention because of the undesirable blurriness of the traditional SR algorithms. Such a side-effect occurs especially when the SR algorithms attempt to minimize distortion-based (or pixel-based) loss function such as mean-squared error (MSE). A model with this objective function tends to have a high peak signal-to-noise ratio (PSNR) and structural similarity (SSIM) [9], but its ability to restore high-frequency details is limited. Thus, the outputs of pixel-oriented models usually disagree with the subjective evaluation scores given by human judges. To improve the human-visual quality, several methods optimize their networks in a perceptual manner. Starting with SRGAN [10], most of the models that aim for good perceptual quality employ the generative adversarial network (GAN) [11] paradigm and perceptual loss [12] instead of pixel-based losses.

However, the most recent methods still fail to fully recover the details on the HR images. Furthermore, we also believe that there is plenty of room to improve such models in an efficiency perspective similar to the traditional SR. To handle

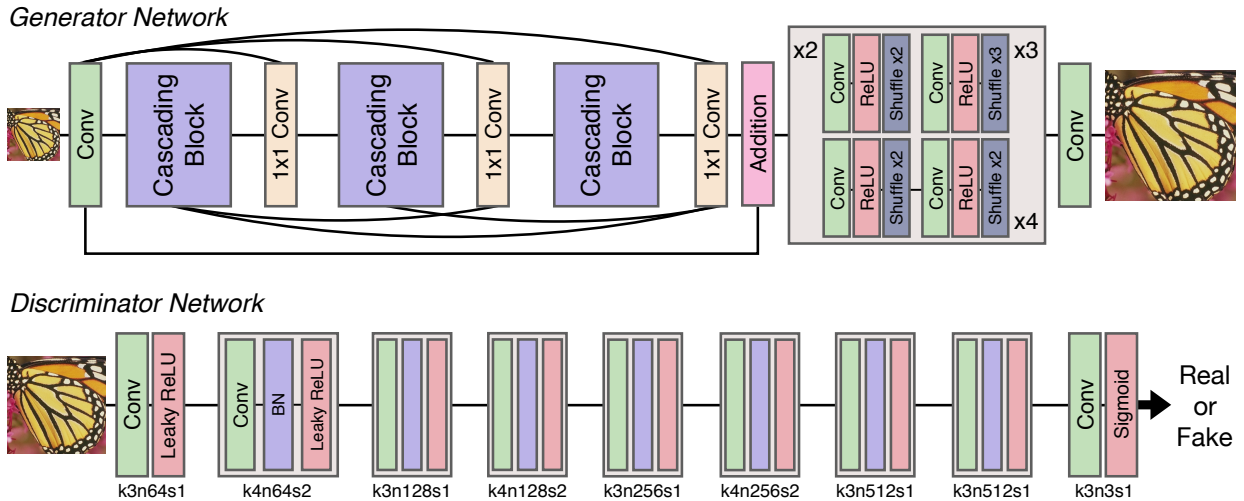


Fig. 1. **Network architecture.** (top) Generator network. This network consists of cascading blocks and upsample blocks. (bottom) Discriminator network with corresponding kernel size (k), number of feature map (n) and stride (s) indicated for each convolution layer.

these requirements and improve the recent models, we propose a photo-realistic cascading residual network (PCARN), which is an extended version of our preliminary work [13]. Following the ESPCN [14], the PCARN family takes the LR images and computes the HR counterparts as the output of the network. In the middle of our networks, we follow the design choice of ResNet [15] that is widely used in recent SR models [10], [16]. Based on this architecture, we introduce a cascading mechanism at both the local and the global levels to incorporate the features from multiple layers. It has the effect of reflecting various levels of input representations in order to receive more information that can be used in the restoration process. For the photo-realistic SR, we adopt a GAN-based training procedure and a multi-scale discriminator which uses discriminators with different scales to improve the ability to preserve the details. Furthermore, as in our prior work [13], we build the PCARN-M (mobile) to allow the users to tune the trade-off between the performance and the heaviness of the model. It is implemented by using the efficient residual block (EResidual) and recursive network scheme.

In summary, our contributions are as follows: **1)** We propose PCARN, a neural network model based on the novel cascading modules that can effectively boost the performance via multi-level representation and multiple shortcut connections. **2)** With GAN-based learning and a multi-scale discriminator, our model can capture fine details effectively. **3)** We also propose PCARN-M for efficient SR by combining the efficient residual block and the recursive network scheme. **4)** Experimental results demonstrate that our method is substantially faster and more lightweight than the recent deep learning-based methods for both distortion- and perceptual-based tasks.

II. RELATED WORK

Single-image super-resolution has been extensively studied in the literature. Here, we first focus on the deep learning-based SR models in Sec. II-A. In Sec. II-B, we discuss recent studies to make a photo-realistic super-resolution model that

has attracted increasing interest recently. Finally, we briefly review the model compression approaches in Sec. II-C.

A. Deep Learning-based SR

Recently, the performance of the SR has been greatly improved with powerful capabilities of the deep learning-based methods. As a pioneer work, Dong et al. [1] propose a deep learning-based model SRCNN that works much better than the traditional algorithms. However, SRCNN requires large computation resources compared to its depth, since the model takes upsampled images as an input. On the other hand, FSRCNN [17] and ESPCN [14] get LR images and upsample the output at the end of the network. This strategy reduces the computation substantially compared to the *early-upsample* scheme. However, the performance could be degraded since most of the recovering processes are done in the LR space. Another issue is that it is tricky to apply the multi-scale training [2] because of the resolution-mismatch problem between the input images across the different scale factors.

However, the aforementioned methods have only a few convolutional layers because of the instability and difficulty of training. To tackle this issue, VDSR [2] introduces global residual learning and shows significant improvement over the previous methods by using 20 convolutional layers. The global residual learning maps the LR images \mathbf{x} to their residual images \mathbf{r} . Then, it produces the SR images \mathbf{y} by adding the residual back into the original, *i.e.*, $\mathbf{y} = \mathbf{x} + \mathbf{r}$. This paradigm facilitates training a deep model with fast and stable convergence. Another approach is progressive upsampling [3], [18], [19], which upsamples the intermediary features periodically to restore the image details gradually. By doing so, those methods effectively perform SR on extremely low-resolution cases compared to the one-stage upsampling manner.

One possible issue of applying a deep learning-based method is the efficiency of the model. To address this concern, most of the previous studies aim to build a lightweight model in terms of parameters. For example, DRCN [7] and DRRN [8]

use a recursive network to reduce the number of parameters so that the model training is much easier even with the limited data. Similarly, MemNet [20] has recursive units in the memory block to boost the performance with only a small number of parameters. This idea is applied to the progressive model as well. The MSLapSRN [21] improves LapSRN [3] by tying the parameters of each feature-embedding blocks and results in the superior performance to the LapSRN.

However, many of the parameter-efficient methods use very deep networks to compensate for degraded performance caused by the use of the recursive scheme and thus require heavy computing resources. We argue that there is a trade-off between performance and efficiency, and aim to build a model that is lightweight in both size and computational aspect.

B. Photo-realistic SR

Generally, deep learning-based SR models are trained using distortion-based (or pixel-based) loss functions (*e.g.*, MSE or L1 loss). The network with these objectives can be optimized easily, but it tends to create blurry artifacts and fails to recover the details such as object edges. This characteristic can be problematic since a human can judge the absence of high-frequency information effortlessly [10]. Hence, to overcome the inherent issue of using distortion-based losses, a generative adversarial network [11] has been adopted to the SR field [10] recently. By doing so, GAN-based methods show promising results in preserving human-perceptive quality. However, since using only an adversarial loss makes the training process unstable, most of the GAN-based models are trained with the addition of pixel losses, despite its downsides. To overcome the inherent problems of pixel losses, Johnson et al. [12] introduces the perceptual loss that calculates the distance between the embedded features of two images.

Besides the SRGAN, many recent works [22]–[24] try to improve the perceptual quality. The EnhanceNet [22] and TSRN [23] adopt texture-matching loss [25] in combination with an adversarial training and perceptual losses. Texture-matching loss was originally used in the texture synthesis problem. Given a target texture image, it generates the output image by iteratively matching the statistics extracted from a pretrained network to the target texture. By using texture information in the SR problem, the model can produce more realistic textures and reduce artifacts. On the other hand, ESRGAN [24] improves the SRGAN in a different direction. Internally, ESRGAN replaces standard residual units with the residual-in-residual dense block (RRDB) inspired by the SRDenseNet [26] and RDN [27]. Then it adds the relative discriminator loss [28] to increase the visual quality. However, perceptually-oriented models are not suitable for the real world applications despite the fascinating performances. On the contrary, our proposed models create photo-realistic images with a reasonable amount of computation in order to suit the real-world demands.

For the photo-realistic SR task, how to measure the quality is a major argument. There are many studies that propose distortion-based metrics for the image quality assessment [9], [29], [30]. But these works do not always reflect the vi-

sual quality, and some metrics often contradict human judgment [10]. Blau et al. [31] reveal the trade-off between the average distortion and perceptual quality. Considering the trade-off, we mainly use NIMA [32] and LPIPS [33] perceptual quality metrics as our benchmark test. The NIMA is a newly proposed metric that predicts the distribution of human opinion scores using a deep learning model. It makes the assessment in a non-reference, where all the evaluation is done without ground-truth images. The LPIPS criticizes the perceptual quality by using the distance between two deep features generated by the network pretrained on ImageNet [34]. Upon the pretrained network, they add an extra linear layer and fine-tune it to the human perceptual dataset. In our experiments, we use a fine-tuned AlexNet (linear version 0.1) [35].

C. Efficient Neural Network

There has been rising interest in building a small and efficient network [5], [36]–[38]. These approaches can be categorized into three groups: **1)** Compressing pretrained networks using pruning or quantizing techniques, **2)** transferring knowledge of a deep model to shallow one, and **3)** designing small but efficient models. In this section, we summarize the latter category, which aims to build a lean neural network in terms of design engineering.

Iandola et al. [6] introduces SqueezeNet to build a parameter-efficient architecture based on the AlexNet [35]. By doing so, they achieve comparable performance level with $50\times$ fewer parameters than the baseline model. Unlike the SqueezeNet, MobileNet [36] aims to decrease the number of operations in order to reduce the inference runtime. This model decomposes the standard convolution to the 1×1 and depth-wise separable convolution used in the previous studies [39], [40]. While the MobileNet cuts down the computational cost effectively, 1×1 convolution becomes the new bottleneck and thus can be the limitation to pushing down the overall cost. To mitigate this issue, ShuffleNet variants [41], [42] use the channel shuffle unit following the 1×1 group convolution. Referring to the recent literature, we apply a depthwise separable convolution technique in the residual block with a generalized form to achieve a fast and lightweight SR model.

III. OUR METHODS

Our proposed photo-realistic cascading residual network (PCARN) is built on our prior model, CARN [13]. In Sec. III-A, we explain the concept of our CARN and PCARN. Then, we introduce the work extending the photo-realistic SR in Sec. III-B. Finally, PCARN-M is shown in Sec. III-C.

A. Cascading Residual Network

Our proposed PCARN is based on CARN, which is in turn based on the ResNet [43]. The prime difference between ResNet and our model is the presence of local and global cascading modules. Fig. 1 (top) graphically depicts how the global cascading occurs. The outputs of intermediary features are cascaded into the higher blocks and finally converge on a single 1×1 convolution layer. Note that the intermediary

modules are implemented as a cascading block, which also hosts cascading connections themselves in a local way. Such local cascading operations are shown in Figure 2, which shows that the local connection is almost identical to a global one, except that the backbone units are the residual blocks.

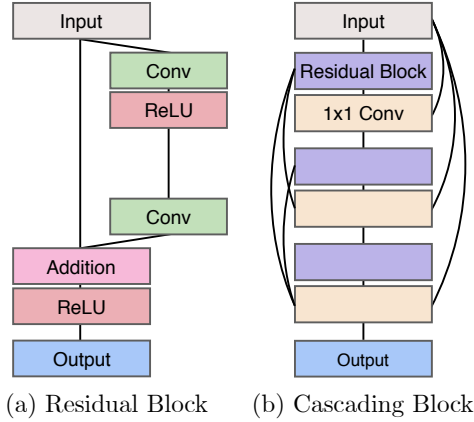


Fig. 2. **Structures of local blocks.** (a) Residual block. (b) Cascading block composed of residual blocks and local cascading connections.

To express how cascading works formally, let f be a convolution layer and τ be a nonlinearity, ReLU in our case. Now we can define the i -th residual block R_i , which has two convolutions followed by an additive operation, as

$$R_i(H^{i-1}; W_R^i) = \tau(f(\tau(f(H^{i-1}; W_R^{i,1})); W_R^{i,2}) + H^{i-1}). \quad (1)$$

Here, H^i is the output of the i -th residual block, W_R^i is the parameter set of the residual block, and $W_R^{i,j}$ is the parameter of the j -th convolution layer in the i -th block. With these notations, we denote the output feature of the final residual block of ResNet as H^u and it becomes the input to the upsampling block. Note that since our model has an entry convolution layer, the first residual block takes $f(\mathbf{X}; W_c)$ as input, where W_c is the parameter of the convolution layer.

$$H^u = R_u(\dots(R_1(f(\mathbf{X}; W_c); W_R^1))\dots; W_R^u). \quad (2)$$

As mentioned above, we replace the standard residual block with the local cascading block that is shown in Fig. 2 (b). To formulate the local cascading as well, we denote $B^{i,j}$ as the output of the j -th residual block in the i -th cascading block, and W_c^i as the set of parameters of the i -th local cascading block. Then, the i -th local cascading block B_{local}^i is defined as in Equation 3.

$$B_{local}^i(H^{i-1}; W_l^i) \equiv B^{i,U}, \quad (3)$$

where $B^{i,U}$ is defined recursively from the $B^{i,u}$'s as:

$$\begin{aligned} B^{i,0} &= H^{i-1} \\ B^{i,u} &= f([I, B^{i,0}, \dots, B^{i,u-1}, R^u(B^{i,u-1}; W_R^u)]; W_c^{i,u}) \\ &\text{for } u = 1, \dots, U. \end{aligned}$$

Finally, we define the output feature of the final cascading block H^b by combining both the local and the global cascading with H^0 , the output of the entry layer.

$$\begin{aligned} H^0 &= f(\mathbf{X}; W_c) \\ H^b &= f([H^0, \dots, H^{b-1}, B_{local}^u(H^{b-1}; W_B^b)]) \\ &\text{for } b = 1, \dots, B. \end{aligned} \quad (4)$$

On top of our preliminary work [13], we modify the model to boost up the performance. There are two main approaches we take to achieve this.

First, inspired by the VDSR [2], we attach global residual learning in our framework. To do that, we aggregate the output of the entry layers and the final 1×1 convolution layer right before the upsampling block. Formally, it can be written as

$$O = H^b + H^0, \quad (5)$$

the final feature map O becomes the input to the upsampling block. This effect of the final addition might appear to be duplicated, since the output of the first convolution is already added to the 1×1 before being added again in the next step. Nonetheless, we found that this duplicate addition is favorable for the overall performance with little computational overhead.

Second, unlike the CARN, we adjust the positions of the nonlinearities in the network. That is, we eliminate the nonlinearities following the 1×1 convolution layer. This is because we want to facilitate the information flow, which CARN is known to suffer from. Additionally, we attach additional nonlinearities in the upsampling unit in order to increase the expressive power of the network.

By applying the cascading mechanism on the local and global levels, we can get two advantages: **1)** The model incorporates features from multiple layers, which allows learning a multi-level representation. **2)** The multi-level cascading connection operates as a multi-level shortcut connection that easily propagates information from lower to higher layers (and vice-versa, in the case of back-propagation). The multi-level representation we are using is similar to the one used in recent work [44], [45], but we apply this arrangement to a variety of feature levels, as shown in Equation 4. Hence, the model can reconstruct the LR image based on multi-level features, and the upsampling unit also upsamples images by consulting the diverse features. Thus, this attribute helps the model restore the details and contexts of the image simultaneously.

B. Photo-realistic Cascading Residual Network

Following Goodfellow et al. [11], we define a discriminator network D , which we optimize in an alternative procedure along with the PCARN network G . Using the discriminator and PCARN generator, we denote the adversarial loss as:

$$\begin{aligned} L_{GAN}(G, D) &= \mathbb{E}_{I_{HR}} [\log D(I_{HR})] + \\ &\quad \mathbb{E}_{I_{LR}} [\log(1 - D(G(I_{LR})))] , \end{aligned} \quad (6)$$

where I_{HR} and I_{LR} denote the HR and LR images, respectively. The idea of adversarial loss is that it trains the generative model G to fool the discriminator D , whereas the

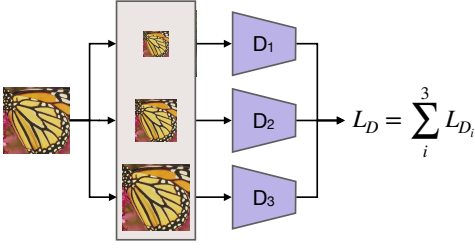


Fig. 3. **Conceptual illustration of the multi-scale discriminator.** Input image is downsampled using average pooling and each image is taken by the corresponding scale discriminator. Total discriminative loss is calculated by summing over all the scale losses.

discriminator is trained to distinguish whether the images are from the SR or the HR sets. This formulation encourages the generator to create perceptually superior images compared to the pixel-based (distortion-based) losses. This is contrary to the distortion-based SR solutions, which are obtained by minimizing pixel-wise error metrics, such as the MSE.

Many previous works have mixed the adversarial loss with a traditional pixel-based loss to stabilize the training process [46], [47]. In this case, the task of a generator is not only to fool the discriminator but also to create an SR image similar to the HR. We also take this option but use the VGG loss instead of the pixel-based loss to avoid the blurring artifact. The VGG loss function [10], [12] is the distance between the outputs of the ReLU layer of the pre-trained VGGNet [48]. Formally, we denote the output feature map of the j -th nonlinearity following convolution layer before the i -th pooling layer as $\phi_{i,j}$. Then, we define the VGG loss as the L2 distance between the feature representation of the HR image I_{HR} , and the super-resolved image $G(I_{LR})$:

$$L_{VGG}(G) = \frac{1}{W_{i,j} H_{i,j}} \sum_x \sum_y^{W_{i,j} H_{i,j}} [\phi_{i,j}(I_{HR})_{x,y} - \phi_{i,j}(G(I_{LR}))_{x,y}]^2. \quad (7)$$

Here, $W_{i,j}$ and $H_{i,j}$ are the spatial resolutions of the feature map. In our work, we use $i = j = 5$.

To improve the fine details of computed outputs, we use the multi-scale discriminator as depicted in Fig. 3. The main idea is to use the multiple discriminators instead of just one and to make each discriminator handle a specific scale. To do so, we downsample the input of the discriminators using average pooling and calculate the total discriminator loss by summing the individual losses. Using this idea allows us gather information across coarse- to fine-resolution images.

C. Efficient Photo-realistic Cascading Residual Network

To improve the efficiency of PCARN, we propose an efficient residual and cascading block. This approach is analogous to the MobileNet [36], but we use group convolution instead of depthwise separable convolution. Our efficient residual (EResidual) block is composed of two consecutive 3×3 group convolutions and a single pointwise convolution, as shown in Fig. 4 (a). The advantage of using group convolution over the

depthwise separable convolution is that it makes the efficiency of the model tunable. Thus, a user can choose the group size to be appropriate for the demand of their desired performance since the number of the group and the performance are in a trade-off relationship. In addition, we examine that depthwise separable convolution extremely degrades the performance. We argue that this is because the number of channels of convolution layers of our models is marginally smaller than that used in MobileNet, so entirely decoupling the spatial and the channel-wise viewpoint can be risky.

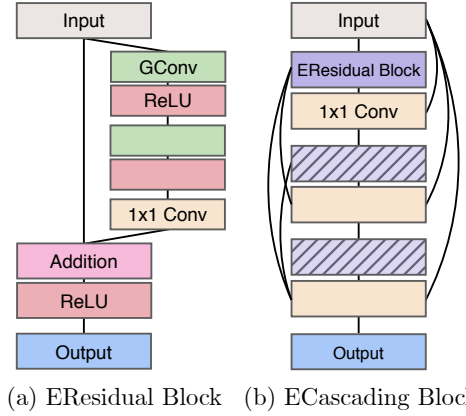


Fig. 4. **Simplified structures of efficient cascading blocks.** (a) Efficient residual block, and (b) is the efficient cascading block. Hatched boxes in (b) denote the residual block with a parameter tying.

The analysis of the cost efficiency of using the EResidual block is as follows. Let K be the kernel size and C_{in}, C_{out} be the number of input and output channels. Since we retain the spatial resolution of the feature map by the padding, we can denote F to be both the input and output feature size. Then, the cost of a standard residual block is

$$2 \times (K^2 \cdot C_{in} \cdot C_{out} \cdot F^2). \quad (8)$$

Note that we exclude the cost of the addition or nonlinearity, and consider only the convolution layers. It is because both the standard and the efficient blocks have the same number of such modules and these operations occupy a negligible portion of the entire computational cost.

Let G be the group size. Then, the cost of an EResidual block, which consist of two group convolutions and one 1×1 convolution, is as given in Equation 9.

$$2 \times \left(K^2 \cdot C_{in} \cdot \frac{C_{out}}{G} \cdot F^2 \right) + C_{in} \cdot C_{out} \cdot F^2 \quad (9)$$

Hence, by changing a standard residual block to our efficient block, we can reduce the computation by the ratio of

$$\frac{2 \times \left(K^2 \cdot C_{in} \cdot \frac{C_{out}}{G} \cdot F^2 \right) + C_{in} \cdot C_{out} \cdot F^2}{2 \times (K^2 \cdot C_{in} \cdot C_{out} \cdot F^2)} = \frac{1}{G} + \frac{1}{2K^2}. \quad (10)$$

Because we use a kernel size as 3×3 for all convolutional layers, and the number of the channels is constant (*i.e.* 64)

except the entry, exit, and upsampling block, the EResidual block reduces the computation from 1.8 up to 14 times depending on the group size. To find the best trade-off between performance and computation, we perform an extensive case study in Section IV-C. To further reduce the parameters, we apply a technique similar to the one used by the recursive network. In other words, we force the EResidual block to be shared in the cascading block, so only one-third of the parameters are needed compared to the standard block. Fig. 4 (b) shows our efficient cascading block after applying the recursive scheme. The solid color boxes illustrate the standard modules and the hatched ones show shared components.

D. Comparison to Recent Models

1) *Comparison to MemNet*: Although MemNet [20] and ours have similar motivation, there are two main distinctions from our schemes. **1)** Feature fusion is done in a different location and manner. For instance, MemNet fuses the output features of each recursive unit at the end of the memory blocks. On the other hand, we gather the information at every possible site in the local block, thus can boost up the representation power via additional layers. **2)** MemNet takes an *early-upsample* approach which upsamples the image before putting it on the model. Although it becomes easier to implement residual learning, it worsens the model efficiency substantially. In contrast, our model gets LR images and intermediate features are upsampled at the end of the network, which enables us to accomplish a good balance between performance and efficiency.

2) *Comparison to DenseNet Variants*: SRDenseNet [26] and RDN [27] use a densely connected block and skip connection. Although the overall design concept can be similar, our model has two main advantages. **1)** In our models, the output of each block is associated with a global cascading connection which is a generalized form of the skip connection. In SRDenseNet and RDN, all levels of features are combined after the final dense block, but our global cascading scheme connects all blocks, which behaves as a multi-level skip connection. **2)** The connectivity schemes that we use are economical for both memory and speed. In a densely connected block, output features are concatenated to the previous information and merged at the end of the block. Because of the nature of this block, SRDenseNet and RDN require a huge burden of computation cost. In contrast, we incorporate features using an additional 1×1 convolution layer at each concatenation point, which facilitates composing more lightweight models.

E. Implementation Details

In the proposed PCARN variants, we set both B and U as three, 64 for the number of channels in all convolutional layers except for the first, last and upsample layers. To upsample the features, we adopt the pixelshuffle layer used in ESPCN. We train our models with the ADAM optimizer [49] by setting $\beta_1 = 0.9$, $\beta_2 = 0.999$, and $\epsilon = 10^{-8}$ in 6×10^5 steps. The minibatch size is 64, and the learning rate begins at 10^{-4} and is halved every 4×10^5 steps.



Fig. 5. **Visual comparison of adversarial training.** We compare the results trained with (PCARN) and without the adversarial training (PCARN-L1).

For the pixel-based PCARN, we use the L1 loss as our loss function instead of the L2. The L2 loss is widely used in the image restoration task because of its relationship to the peak signal-to-noise ratio (PSNR). However, in our experiments, L1 provided better convergence and performance. To train the GAN-based PCARN, we employ the pretrained PCARN with L1 loss and fine-tune it for 2×10^5 steps with the same settings as in the above model.

We train the model using the DIV2K dataset [50], which consists of 800 training, 100 validation, and 100 test 2K resolution images. Because of the richness of this dataset, recent SR models [4], [16], [51], [52] use DIV2K as well. To prepare the training input, we randomly crop images to the 48×48 LR patches and augment to horizontal flip or rotation. For the test and benchmark, Set5 [53], Set14 [54], B100 [55] and Urban100 [56] datasets are used. To enable the multi-scale training, we construct the training batch using a scale of either 2 or 4, since our model can process only a single scale for each batch. The code is publicly available online on <https://github.com/nmhkahn/PCARN-pytorch>.

IV. EXPERIMENTAL RESULTS AND DISCUSSIONS

In this section, we first present the analysis results of our model. Then, we will show the quantitative evaluation of the distortion-based and perception-based models. Finally, we will illustrate the visual comparison and limitations. For all the model analysis part (Sec. IV-A~IV-C), we conduct experiments with a 32×32 LR patch size running 4×10^5 steps. Furthermore, we train and evaluate each of the methods ten times to inspect the performance more accurately. One thing to note here is that we represent the number of operations by Mult-Adds. It is the number of composite multiply-accumulate operations for a single image. We assume the HR image to be 720p (1280×720) to calculate Mult-Adds.

We use various metrics to evaluate the performance. For the distortion-based comparison, PSNR and SSIM [9] are used. The perception-based performance is measured by the LPIPS [33] and NIMA [32] scores. We use the LPIPS settings of the AlexNet with the fine-tuned linear layer (AlexNet-linear, version 0.1), and MobileNet for the NIMA backbone model.

A. Model Design Analysis

To investigate the performance of the proposed methods, we analyze our models via ablation study. We select the baseline

to be the SRResNet. Other models have the same topologies except for the inherent modules (such as the additional 1×1 convolution) that are needed for each particular architecture. Thus, the overall number of parameters is increased by up to 15% from the baseline to our final model. Table I shows the model analysis on the effect of cascading modules and the global residual learning paradigm.

TABLE I
ANALYSIS OF THE EFFECT OF MODEL DESIGN CHOICES.

| Model | Params | PSNR | SSIM |
|------------|--------|-------------------|--------------------|
| Baseline | 963K | 28.42±0.02 | 0.7773±3e-4 |
| + Local | 1,074K | 28.45±0.01 | 0.7780±3e-4 |
| + Global | 1,000K | 28.47±0.02 | 0.7787±4e-4 |
| CARN | 1,111K | 28.49±0.02 | 0.7788±3e-4 |
| + Residual | 1,111K | 28.50±0.01 | 0.7792±3e-4 |

We see that the model with local cascading works better than the baseline since this scheme carries mid- to high-level frequency signals inside the block more fluently. Moreover, this approach conveys not only the inputs but also the mixture of intermediate features to the next block, which leverages the multi-level representations. By incorporating multi-level representations, the model can consider a variety of information from many different receptive fields when reconstructing the image. We observed higher performance gain with the global cascading scheme. This is because the advantages of the local scheme are limited to each block, which lessens the model’s ability to exploit the cascading effect. One major benefit of the global cascading is that it allows for information integration from lower layers, and this information shortcut provides useful clues needed to reconstruct the HR image in the upsampling and final reconstructing processes.

In addition to CARN, we employ the global residual learning scheme shown in many recent SR methods [2], [16]. The benefit of using it is minor compared to the CARN itself, since the roles of the global cascading and residual learning overlap. However, we choose CARN with residual learning as our PCARN model since it does improve performance with negligible overhead to the operation size.

TABLE II
MODEL ANALYSIS STUDY ON PERCEPTUAL PERSPECTIVE. MSD INDICATES PCARN WITH MULTI-SCALE DISCRIMINATOR.

| Model | LPIPS | PSNR | SSIM |
|----------|--------------------|------------|-------------|
| PCARN-L1 | 0.2888±1e-3 | 28.50±0.01 | 0.7792±3e-4 |
| + GAN | 0.1615±5e-3 | 26.36±0.25 | 0.7120±6e-3 |
| + MSD | 0.1547±2e-3 | 26.10±0.17 | 0.6980±8e-3 |

To build a photo-realistic SR model, we must design a well-functioning discriminator. To see how the choice of discriminator affects the overall performance, we conducted a series of comparisons across the various types of discriminator loss. The LPIPS is used to measure the perception quality.

As shown in Table II, PCARN with adversarial training (+GAN) outperforms the baseline by a large margin. Fig. 5

also exhibits the advantage of using GAN, where it successfully recovers the fine details and generates more photo-realistic images. However, since the magnitude of the pixel-level signal is diminished, the performance of pixel-based metrics (PSNR and SSIM) is degraded. Moreover, the overall training process is substantially unstable and shows high variance in all metrics.

Using the multi-scale discriminator (+MSD) also gives an additional gain to the LPIPS. The reasons are two-fold: **1)** Since we use the sum of multiple discriminators as the total loss, the magnitude of the discriminator loss is amplified (compared to averaging them). **2)** The signals of multi-discriminators are well-fused across the different scales, which allows the model to generate detail-preserving output while maintaining the overall structure.

B. Initialization Strategy

Initializing the network in an appropriate manner is the key component for boosting the performance. To verify what is best for our models, we performed an experiment comparing the benchmark to six common initialization schemes: uniform, and normal distribution with various settings, as shown in Table III. Interestingly, the MSRA initialization [57], given by the equation $1.0 \times N(0, \sqrt{2/F})$, and the high-range uniform initialization performed poorly against others. We argue that narrow 1×1 convolution affects the quality of initialization, since the high-variance initial values tend to result in high-variance performance. On the other hand, multiplying 0.1 degrade since it makes the model converge too early.

TABLE III
EFFECT OF THE INITIALIZATION. F DENOTES THE NUMBER OF THE INPUT CHANNELS (FAN-IN). U/N ARE UNIFORM/NORMAL DISTRIBUTION.

| Initialization | PSNR | SSIM |
|-------------------------------|-------------------|--------------------|
| $0.1 \times N(0, \sqrt{2/F})$ | 28.46±0.01 | 0.7781±3e-4 |
| $1.0 \times N(0, \sqrt{2/F})$ | 28.45±0.02 | 0.7777±3e-4 |
| $0.1 \times U(\pm\sqrt{6/F})$ | 28.47±0.01 | 0.7782±3e-4 |
| $1.0 \times U(\pm\sqrt{6/F})$ | 28.44±0.01 | 0.7778±2e-4 |
| $0.1 \times U(\pm\sqrt{1/F})$ | 28.45±0.02 | 0.7775±4e-4 |
| $1.0 \times U(\pm\sqrt{1/F})$ | 28.50±0.01 | 0.7791±3e-4 |

Fig. 6 supports the hypothesis as well. We plot the smoothed histogram of the binned initialized values for various initialization schemes. The gap between the ResNet with MSRA initialization (black solid) and ours (blue dots) is significant. The main reason is the difference in the channel size between the ResNet and ours: our models have considerably fewer channels for all the convolutional layers, which leads to the high standard deviation. In addition, the use of 1×1 convolution intensifies the issue since it has only one-ninths of the input channels compared to the 3×3 layer. The shape of the initialization scheme with $1.0 \times U(\pm\sqrt{1/F})$ (green dash) best matches that of the ResNet.

C. Efficiency Trade-off

Fig. 7 depicts the trade-off analysis between the performance and efficiency of the efficient PCARN that uses convo-

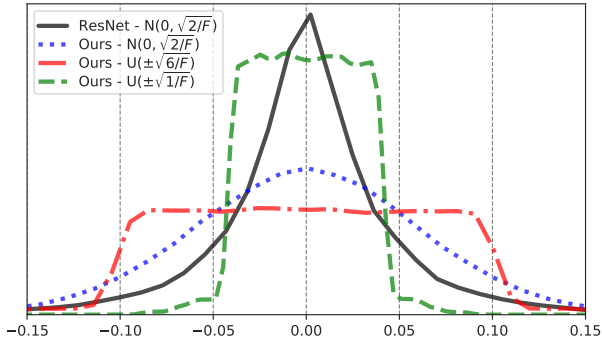


Fig. 6. **Distribution of the randomly initialized networks.** We plot 100K parameters for each model using 1000 bins. Each of the parameter distributions is from the diverse sources because of the variation in the number of input channels.

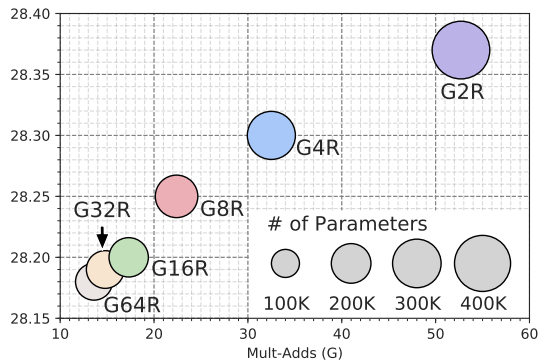


Fig. 7. **Efficiency analysis of efficient models.** We evaluate all models on Set14 with $\times 4$ scale. G represents the group size of the group convolution, and R means the model with the recursive network scheme.

lution and a recursive scheme. Although all efficient models perform worse than the PCARN, the number of parameters and operations are decreased dramatically. We choose $G4R$ as the best-balanced model, which we denote as PCARN-M (mobile), since the effect of compressing the model is reduced after group size is more than four. As a result, PCARN-M reduces the number of parameters by four times and the number of operations by nearly three times with a loss of 0.20 PSNR and 0.0053 SSIM, compared to the PCARN.

D. Quantitative Comparisons

1) *Comparisons with Distortion-based Methods:* Here, we compare the proposed models on distortion-based metrics. Table IV shows the quantitative comparisons of the performances over the various benchmark datasets for the models that have parameters of less than 2,000K. The performance of PCARN exceeds all the previous methods on many benchmark datasets, especially for the $\times 2$ and $\times 3$ cases. The PCARN-M model achieves comparable results using very few operations.

To make our models even more lightweight, we apply the multi-scale learning approach to process multiple scales using a single trained model. This helps us alleviate the burden of heavy-weight model size when deploying the SR application on mobile devices; PCARN(-M) needs only a single fixed

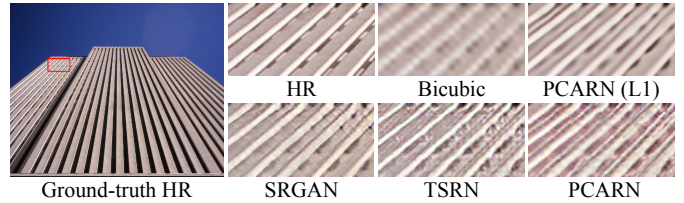


Fig. 8. **A failure case.** Our perception-based model cannot is not able to reconstruct the details without sufficient information when constructing a dense structure.

model for multiple scales, unlike the other state-of-the-art algorithms. This property is well-suited for real-world products because the size of the applications has to be fixed, whereas the scale of given LR images could differ. Using the multi-scale learning for our models increases the number of parameters since the network has to contain possible upsampling layers.

2) *Comparisons with Perception-based Methods:* Tables V and VI depict the quantitative comparisons for the $\times 4$ scale dataset on the perception-based metrics, LPIPS and NIMA respectively. Among the perception-based methods, our PCARN and PCARN-M have the least Mult-Adds and the similar number of parameters with the other algorithms. With the limited resources, our models outperform all the competitors in LPIPS metric and show comparable results on the NIMA score. We also report the perception score on the various scale factors in Table VII. Again, we want to emphasize that our models are capable to take multiple scale factors with a single network. To the best of our knowledge, this characteristic is the first attempt at the perception-based SR task.

E. Visual Comparison with State-of-the-arts

In Fig. 9, we illustrate the qualitative comparisons of the distortion-based methods for the $\times 4$ scale. It can be seen that our models work better than others and accurately reconstructs not only the line patterns (e.g., stairs), but also complex objects such as the facial texture. We also present the results of the perception-based models in Fig. 10. Our methods produce a more photo-realistic texture especially for the fine-details such as lines and furs of the lion. Moreover, the proposed networks also generate more clean outputs while other perception-based methods suffer the visually-implausible artifacts.

Our GAN-based PCARN can produce sharp and realistic images as shown in Fig. 10. However, in some dense structures like Fig. 8, it generates undesirable artifacts, unlike the L1 loss-based PCARN. We suspect that this is a common limitation shared by most, if not all, GAN-based algorithms as well because of the perception-distortion trade-off [31].

V. CONCLUSION

In this work, we proposed a deep convolutional network with a cascading scheme for fast and accurate image super-resolution. The main idea is adding multiple cascading connections starting from each intermediary layer to the others in local and global levels. In addition, we extend our preliminary method [13] to the photo-realistic super-resolution task using a multi-scale discriminator and achieved improved performance



Fig. 9. Visual qualitative comparison between distortion-based methods on the $\times 4$ SR datasets.

over the recent models that have complexity analogous to ours. All the experiments were conducted on the super-resolution field, but we hope that our work can potentially be applied to other image restoration subjects [61] as well.

REFERENCES

- [1] C. Dong, C. C. Loy, K. He, and X. Tang, "Learning a deep convolutional network for image super-resolution," in *Proceedings of the European Conference on Computer Vision (ECCV)*, 2014.
- [2] J. Kim, J. Kwon Lee, and K. Mu Lee, "Accurate image super-resolution using very deep convolutional networks," in *Proceedings of the Conference on Computer Vision and Pattern Recognition (CVPR)*, 2016.
- [3] W.-S. Lai, J.-B. Huang, N. Ahuja, and M.-H. Yang, "Deep laplacian pyramid networks for fast and accurate super-resolution," in *Proceedings of the Conference on Computer Vision and Pattern Recognition (CVPR)*, 2017.
- [4] Y. Zhang, K. Li, K. Li, L. Wang, B. Zhong, and Y. Fu, "Image super-resolution using very deep residual channel attention networks," in *Proceedings of the European Conference on Computer Vision, Munich, Germany*, 2018, pp. 8–14.
- [5] S. Han, H. Mao, and W. J. Dally, "Deep compression: Compressing deep neural networks with pruning, trained quantization and Huffman coding," *Proceedings of the International Conference on Learning Representations (ICLR)*, 2016.
- [6] F. N. Iandola, S. Han, M. W. Moskewicz, K. Ashraf, W. J. Dally, and K. Keutzer, "Squeezenet: Alexnet-level accuracy with 50x fewer parameters and 0.5 mb model size," *arXiv preprint arXiv:1602.07360*, 2016.
- [7] J. Kim, J. Kwon Lee, and K. Mu Lee, "Deeply-recursive convolutional network for image super-resolution," in *Proceedings of the Conference on Computer Vision and Pattern Recognition (CVPR)*, 2016.
- [8] Y. Tai, J. Yang, and X. Liu, "Image super-resolution via deep recursive residual network," in *Proceedings of the Conference on Computer Vision and Pattern Recognition (CVPR)*, 2017.
- [9] Z. Wang, A. C. Bovik, H. R. Sheikh, and E. P. Simoncelli, "Image quality assessment: from error visibility to structural similarity," *IEEE transactions on image processing*, vol. 13, no. 4, pp. 600–612, 2004.
- [10] C. Ledig, L. Theis, F. Huszár, J. Caballero, A. Cunningham, A. Acosta, A. P. Aitken, A. Tejani, J. Totz, Z. Wang *et al.*, "Photo-realistic single image super-resolution using a generative adversarial network," in *Proceedings of the Conference on Computer Vision and Pattern Recognition (CVPR)*, 2017.
- [11] I. Goodfellow, J. Pouget-Abadie, M. Mirza, B. Xu, D. Warde-Farley, S. Ozair, A. Courville, and Y. Bengio, "Generative adversarial nets," in *Advances in neural information processing systems*, 2014, pp. 2672–2680.
- [12] J. Johnson, A. Alahi, and L. Fei-Fei, "Perceptual losses for real-time style transfer and super-resolution," in *European Conference on Computer Vision*. Springer, 2016, pp. 694–711.
- [13] N. Ahn, B. Kang, and K.-A. Sohn, "Fast, accurate, and lightweight super-resolution with cascading residual network," in *Proceedings of the European Conference on Computer Vision (ECCV)*, 2018.
- [14] W. Shi, J. Caballero, F. Huszár, J. Totz, A. P. Aitken, R. Bishop, D. Rueckert, and Z. Wang, "Real-time single image and video super-resolution using an efficient sub-pixel convolutional neural network," in *Proceedings of the Conference on Computer Vision and Pattern Recognition (CVPR)*, 2016.
- [15] K. He, X. Zhang, S. Ren, and J. Sun, "Deep residual learning for image recognition," in *Proceedings of the Conference on Computer Vision and Pattern Recognition (CVPR)*, 2016.
- [16] B. Lim, S. Son, H. Kim, S. Nah, and K. M. Lee, "Enhanced deep residual networks for single image super-resolution," in *Proceedings of the Conference on Computer Vision and Pattern Recognition (CVPR) Workshops*, 2017.
- [17] C. Dong, C. C. Loy, and X. Tang, "Accelerating the super-resolution convolutional neural network," in *Proceedings of the European Conference on Computer Vision (ECCV)*, 2016.
- [18] Y. Wang, F. Perazzi, B. McWilliams, A. Sorkine-Hornung, O. Sorkine-Hornung, and C. Schroers, "A fully progressive approach to single-image super-resolution," in *Proceedings of the IEEE Conference on Computer Vision and Pattern Recognition Workshops*, 2018, pp. 864–873.
- [19] N. Ahn, B. Kang, and K.-A. Sohn, "Image super-resolution via progres-

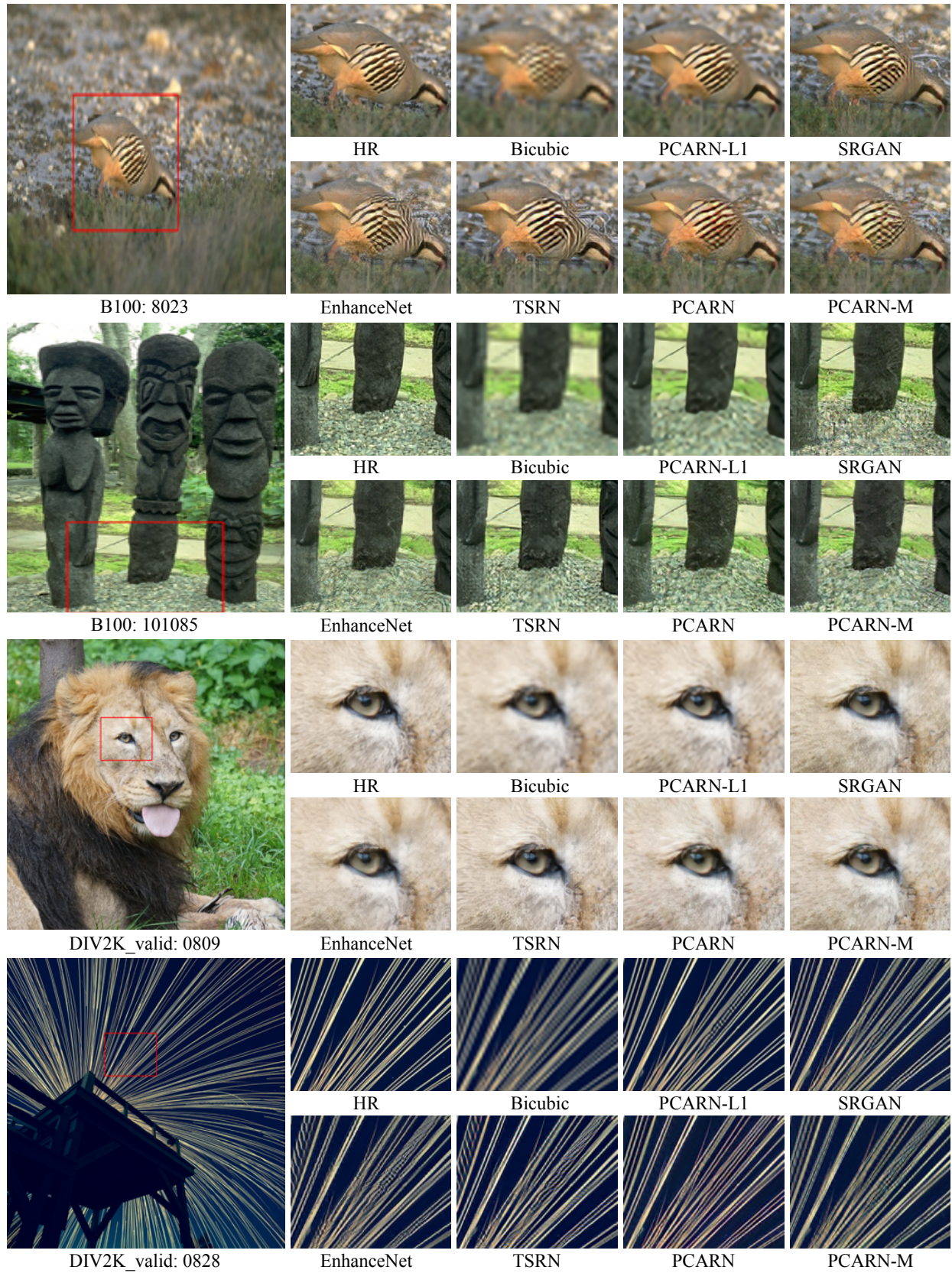


Fig. 10. Visual qualitative comparison between perception-based methods on the $\times 4$ SR datasets.

TABLE IV
RESULTS OF DISTORTION-BASED MODELS. BOLD AND UNDERLINE INDICATE BEST AND SECOND-BEST.

| Scale | Model | Params | MultAdds | Set5 | Set14 | B100 | Urban |
|--------------|-----------------|--------|---------------------|----------------------|---------------------|----------------------|---------------------|
| | | | | PSNR/SSIM | PSNR/SSIM | PSNR/SSIM | PSNR/SSIM |
| 2 | SRCNN [1] | 57K | 52.7G | 36.66/0.9542 | 32.42/0.9063 | 31.36/0.8879 | 29.50/0.8946 |
| | FSRCNN [17] | 12K | 6.0G | 37.00/0.9558 | 32.63/0.9088 | 31.53/0.8920 | 29.88/0.9020 |
| | VDSR [2] | 665K | 612.6G | 37.53/0.9587 | 33.03/0.9124 | 31.90/0.8960 | 30.76/0.9140 |
| | DRCN [7] | 1,774K | 17,974.3G | 37.63/0.9588 | 33.04/0.9118 | 31.85/0.8942 | 30.75/0.9133 |
| | CNF [58] | 337K | 311.0G | 37.66/0.9590 | 33.38/0.9136 | 31.91/0.8962 | - |
| | LapSRN [3] | 813K | 29.9G | 37.52/0.9590 | 33.08/0.9130 | 31.80/0.8950 | 30.41/0.9100 |
| | DRRN [8] | 297K | 6,796.9G | 37.74/0.9591 | 33.23/0.9136 | 32.05/0.8973 | 31.23/0.9188 |
| | BTSRN [59] | 410K | 207.7G | 37.75/- | 33.20/- | 32.05/- | 31.63/- |
| | MemNet [20] | 677K | 2,662.4G | 37.78/0.9597 | 33.28/0.9142 | 32.08/0.8978 | 31.31/0.9195 |
| | MSLapSRN [21] | 222K | 93.6G | 37.78/ 0.9600 | 33.28/0.9150 | 32.05/0.8980 | 31.15/0.9190 |
| | SelNet [60] | 974K | 225.7G | 37.89/0.9598 | 33.61/0.9160 | 32.08/ 0.8984 | - |
| | CARN [13] | 1,592K | 222.8G | 37.76/0.9590 | <u>33.52/0.9166</u> | <u>32.09/0.8978</u> | <u>31.92/0.9256</u> |
| | CARN-M [13] | 412K | 91.2G | 37.53/0.9583 | 33.26/0.9141 | 31.92/0.8960 | 31.23/0.9193 |
| | PCARN (L1) | 1,592K | 222.8G | <u>37.79/0.9592</u> | 33.55/0.9169 | 32.11/0.8983 | 31.96/0.9261 |
| PCARN-M (L1) | 412K | 91.2G | 37.56/0.9583 | 33.26/0.9145 | 31.94/0.8962 | 31.30/0.9194 | |
| 3 | SRCNN [1] | 57K | 52.7G | 32.75/0.9090 | 29.28/0.8209 | 28.41/0.7863 | 26.24/0.7989 |
| | FSRCNN [17] | 12K | 5.0G | 33.16/0.9140 | 29.43/0.8242 | 28.53/0.7910 | 26.43/0.8080 |
| | VDSR [2] | 665K | 612.6G | 33.66/0.9213 | 29.77/0.8314 | 28.82/0.7976 | 27.14/0.8279 |
| | DRCN [7] | 1,774K | 17,974.3G | 33.82/0.9226 | 29.76/0.8311 | 28.80/0.7963 | 27.15/0.8276 |
| | CNF [58] | 337K | 311.0G | 33.74/0.9226 | 29.90/0.8322 | 28.82/0.7980 | - |
| | LapSRN [3] | 813K | 149.4G | 33.82/0.9220 | 29.87/0.8320 | 28.82/0.7980 | 27.07/0.8280 |
| | DRRN [8] | 297K | 6,796.9G | 34.03/0.9244 | 29.96/0.8349 | 28.95/0.8004 | 27.53/0.8378 |
| | BTSRN [59] | 410K | 176.2G | 34.03/- | 29.90/- | 28.97/- | 27.75/- |
| | MemNet [20] | 677K | 2,662.4G | 34.09/0.9248 | 30.00/0.8350 | 28.96/0.8001 | 27.56/0.8376 |
| | MSLapSRN [21] | 222K | 467.8G | 34.06/0.9240 | 29.97/0.8360 | 28.93/0.8020 | 27.47/0.8370 |
| | SelNet [60] | 1,159K | 120.0G | <u>34.27/0.9257</u> | <u>30.30/0.8399</u> | 28.97/0.8025 | - |
| | CARN [13] | 1,592K | 118.8G | <u>34.29/0.9255</u> | <u>30.29/0.8407</u> | <u>29.06/0.8034</u> | <u>28.06/0.8493</u> |
| | CARN-M [13] | 412K | 46.1G | 33.99/0.9236 | 30.08/0.8367 | 28.91/0.8000 | 27.55/0.8385 |
| | PCARN (L1) | 1,592K | 118.8G | 34.35/0.9258 | 30.32/0.8412 | 29.07/0.8039 | 28.08/0.8499 |
| PCARN-M (L1) | 412K | 46.1G | 34.01/0.9234 | 30.12/0.8376 | 28.92/0.8004 | 27.56/0.8382 | |
| 4 | SRCNN [1] | 57K | 52.7G | 30.48/0.8628 | 27.49/0.7503 | 26.90/0.7101 | 24.52/0.7221 |
| | FSRCNN [17] | 12K | 4.6G | 30.71/0.8657 | 27.59/0.7535 | 26.98/0.7150 | 24.62/0.7280 |
| | VDSR [2] | 665K | 612.6G | 31.35/0.8838 | 28.01/0.7674 | 27.29/0.7251 | 25.18/0.7524 |
| | DRCN [7] | 1,774K | 17,974.3G | 31.53/0.8854 | 28.02/0.7670 | 27.23/0.7233 | 25.14/0.7510 |
| | CNF [58] | 337K | 311.0G | 31.55/0.8856 | 28.15/0.7680 | 27.32/0.7253 | - |
| | LapSRN [3] | 813K | 149.4G | 31.54/0.8850 | 28.19/0.7720 | 27.32/0.7280 | 25.21/0.7560 |
| | DRRN [8] | 297K | 6,796.9G | 31.68/0.8888 | 28.21/0.7720 | 27.38/0.7284 | 25.44/0.7638 |
| | BTSRN [59] | 410K | 165.2G | 31.85/- | 28.20/- | 27.47/- | 25.74/- |
| | MemNet [20] | 677K | 2,662.4G | 31.74/0.8893 | 28.26/0.7723 | 27.40/0.7281 | 25.50/0.7630 |
| | MSLapSRN [21] | 222K | 467.8G | 31.74/0.8890 | 28.26/0.7740 | 27.43/0.7310 | 25.51/0.7680 |
| | SelNet [60] | 1,417K | 83.1G | 32.00/0.8931 | 28.49/0.7783 | 27.44/0.7325 | - |
| | SRDenseNet [26] | 2,015K | 389.9G | 32.02/0.8934 | <u>28.50/0.7782</u> | 27.53/0.7337 | <u>26.05/0.7819</u> |
| | CARN [13] | 1,592K | 90.9G | <u>32.13/0.8937</u> | 28.60/0.7806 | 27.58/0.7349 | 26.07/0.7837 |
| | CARN-M [13] | 412K | 32.5G | 31.92/0.8903 | 28.42/0.7762 | 27.44/0.7304 | 25.62/0.7694 |
| PCARN (L1) | 1,592K | 90.9G | 32.17/0.8940 | 28.60/0.7812 | 27.57/0.7353 | 26.07/0.7840 | |
| PCARN-M (L1) | 412K | 32.5G | 31.85/0.8899 | 28.42/0.7765 | 27.43/0.7307 | 25.62/0.7687 | |

sive cascading residual network,” in *The IEEE Conference on Computer Vision and Pattern Recognition (CVPR) Workshops*, June 2018.

[20] Y. Tai, J. Yang, X. Liu, and C. Xu, “Memnet: A persistent memory network for image restoration,” in *Proceedings of the International Conference on Computer Vision (ICCV)*, 2017.

[21] W.-S. Lai, J.-B. Huang, N. Ahuja, and M.-H. Yang, “Fast and accurate image super-resolution with deep laplacian pyramid networks,” *arXiv:1710.01992*, 2017.

[22] M. S. Sajjadi, B. Schölkopf, and M. Hirsch, “Enhancenet: Single image super-resolution through automated texture synthesis,” in *Proceedings of the International Conference on Computer Vision (ICCV)*, 2017.

[23] M. W. Gondal, B. Schölkopf, and M. Hirsch, “The unreasonable effectiveness of texture transfer for single image super-resolution,” *arXiv preprint arXiv:1808.00043*, 2018.

[24] X. Wang, K. Yu, S. Wu, J. Gu, Y. Liu, C. Dong, C. C. Loy, Y. Qiao, and X. Tang, “Esrgan: Enhanced super-resolution generative adversarial networks,” *arXiv preprint arXiv:1809.00219*, 2018.

[25] L. A. Gatys, A. S. Ecker, and M. Bethge, “Image style transfer using convolutional neural networks,” in *Proceedings of the IEEE Conference on Computer Vision and Pattern Recognition*, 2016, pp. 2414–2423.

[26] T. Tong, G. Li, X. Liu, and Q. Gao, “Image super-resolution using dense skip connections,” in *Proceedings of the International Conference on Computer Vision (ICCV)*, 2017.

[27] Y. Zhang, Y. Tian, Y. Kong, B. Zhong, and Y. Fu, “Residual dense network for image super-resolution,” in *The IEEE Conference on Computer Vision and Pattern Recognition (CVPR)*, 2018.

[28] A. Jolicœur-Martineau, “The relativistic discriminator: a key element missing from standard gan,” *arXiv preprint arXiv:1807.00734*, 2018.

[29] Z. Wang, E. P. Simoncelli, and A. C. Bovik, “Multiscale structural similarity for image quality assessment,” in *The Thirty-Seventh Asilomar*

TABLE V
COMPARISON FOR $\times 4$ SISR ON LPIPS METRIC (ALEXNET-LINEAR VERSION 0.1). LOWER SCORE IS BETTER.

| Model | Params | MultAdds | Set5 | Set14 | B100 | Urban |
|---------------|--------|----------|------------------------|------------------------|------------------------|------------------------|
| SRCNN [1] | 57K | 52.7G | 0.2010 | 0.3145 | 0.4103 | 0.3161 |
| MSLapSRN [21] | 222K | 435.9G | 0.1777 | 0.2988 | 0.3893 | 0.2522 |
| CARN [13] | 1,589K | 90.9G | 0.1767 | 0.2903 | 0.3814 | 0.2366 |
| SRResNet [10] | 1,543K | 127.8G | 0.1729 | 0.2839 | 0.3753 | 0.2259 |
| PCARN (L1) | 1,589K | 90.9G | 0.1769 | 0.2879 | 0.3780 | 0.2350 |
| PCARN-M (L1) | 412K | 32.5G | 0.1793 | 0.3846 | 0.2928 | 0.2528 |
| SRGAN [10] | 1,543K | 127.8G | 0.0881 | 0.1741 | 0.2028 | 0.1558 |
| ENet [22] | 1,073K | 120.6G | 0.0994 | 0.1620 | 0.2102 | 0.1708 |
| TSRN-S [23] | 1,073K | 120.6G | 0.0906 | 0.1478 | 0.2027 | 0.1544 |
| TSRN-G [23] | 1,073K | 120.6G | 0.0881 | 0.1549 | 0.1962 | 0.1537 |
| PCARN | 1,589K | 90.9G | 0.0745 | 0.1449 | 0.1875 | 0.1521 |
| PCARN-M | 412K | 32.5G | 0.0796 | 0.1502 | 0.1981 | 0.1671 |

TABLE VI
COMPARISON FOR $\times 4$ SISR ON NIMA METRIC (MOBILENET). HIGHER SCORE IS BETTER.

| Model | Params | MultAdds | Set5 | Set14 | B100 | Urban |
|---------------|--------|----------|--|--|--|--|
| SRCNN [1] | 57K | 52.7G | 4.316 \pm 1.629 | 4.372 \pm 1.694 | 4.340 \pm 1.695 | 4.624 \pm 1.642 |
| MSLapSRN [21] | 222K | 435.9G | 4.669 \pm 1.583 | 4.797 \pm 1.660 | 4.609 \pm 1.659 | 5.039 \pm 1.602 |
| CARN [13] | 1,589K | 90.9G | 4.731 \pm 1.564 | 4.908 \pm 1.639 | 4.694 \pm 1.640 | 5.149 \pm 1.599 |
| SRResNet [10] | 1,543K | 127.8G | 4.743 \pm 1.574 | 4.910 \pm 1.643 | 4.685 \pm 1.643 | 5.135 \pm 1.599 |
| PCARN (L1) | 1,589K | 90.9G | 4.750 \pm 1.567 | 4.907 \pm 1.639 | 4.704 \pm 1.639 | 5.146 \pm 1.599 |
| PCARN-M (L1) | 412K | 32.5G | 4.708 \pm 1.573 | 4.856 \pm 1.645 | 4.656 \pm 1.643 | 5.092 \pm 1.598 |
| SRGAN [10] | 1,543K | 127.8G | 4.865 \pm 1.560 | 5.002 \pm 1.616 | 4.936 \pm 1.634 | 5.191 \pm 1.590 |
| ENet [22] | 1,073K | 120.6G | 4.859 \pm 1.584 | 5.127 \pm 1.635 | 5.067 \pm 1.649 | 5.201 \pm 1.594 |
| TSRN-S [23] | 1,073K | 120.6G | 4.798 \pm 1.591 | 5.071\pm1.630 | 4.841 \pm 1.660 | 5.143 \pm 1.596 |
| TSRN-G [23] | 1,073K | 120.6G | 5.052\pm1.569 | 5.219\pm1.609 | 5.168\pm1.613 | 5.273\pm1.581 |
| PCARN | 1,589K | 90.9G | 4.929\pm1.534 | 5.063 \pm 1.603 | 5.077\pm1.611 | 5.243\pm1.581 |
| PCARN-M | 412K | 32.5G | 4.865 \pm 1.533 | 4.981 \pm 1.611 | 5.010 \pm 1.616 | 5.180 \pm 1.578 |

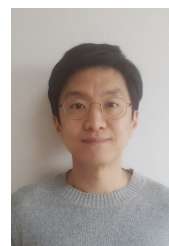
TABLE VII
RECORDS OF OUR MODELS IN DIVERSE SCALES ON LPIPS AND NIMA METRICS.

| Scale | Model | Set5 | Set14 | B100 | Urban |
|-------|--------------|----------------------------|----------------------------|----------------------------|----------------------------|
| | | LPIPS / NIMA | LPIPS / NIMA | LPIPS / NIMA | LPIPS / NIMA |
| 2 | PCARN (L1) | 0.0546 / 4.669 \pm 1.592 | 0.0939 / 4.873 \pm 1.645 | 0.1455 / 4.719 \pm 1.653 | 0.0665 / 5.121 \pm 1.597 |
| | PCARN-M (L1) | 0.0549 / 4.647 \pm 1.595 | 0.0961 / 4.844 \pm 1.649 | 0.1459 / 4.712 \pm 1.653 | 0.0748 / 5.089 \pm 1.598 |
| | PCARN | 0.0187 / 4.872 \pm 1.547 | 0.0453 / 5.118 \pm 1.615 | 0.0598 / 4.980 \pm 1.634 | 0.0400 / 5.240 \pm 1.586 |
| | PCARN-M | 0.0227 / 4.845 \pm 1.575 | 0.0487 / 5.044 \pm 1.628 | 0.0643 / 4.936 \pm 1.641 | 0.0468 / 5.204 \pm 1.585 |
| 3 | PCARN (L1) | 0.1251 / 4.685 \pm 1.585 | 0.2097 / 4.828 \pm 1.636 | 0.2863 / 4.646 \pm 1.645 | 0.1612 / 5.108 \pm 1.592 |
| | PCARN-M (L1) | 0.1278 / 4.656 \pm 1.585 | 0.2144 / 4.773 \pm 1.639 | 0.2908 / 4.619 \pm 1.647 | 0.1769 / 5.060 \pm 1.592 |
| | PCARN | 0.0437 / 4.867 \pm 1.542 | 0.0962 / 5.122 \pm 1.601 | 0.1294 / 5.042 \pm 1.623 | 0.0951 / 5.210 \pm 1.576 |
| | PCARN-M | 0.0528 / 4.787 \pm 1.557 | 0.1061 / 5.003 \pm 1.604 | 0.1386 / 4.948 \pm 1.629 | 0.1076 / 5.170 \pm 1.575 |
| 4 | PCARN (L1) | 0.1769 / 4.750 \pm 1.567 | 0.2879 / 4.907 \pm 1.639 | 0.3780 / 4.704 \pm 1.639 | 0.2350 / 5.146 \pm 1.599 |
| | PCARN-M (L1) | 0.1793 / 4.708 \pm 1.573 | 0.3846 / 4.856 \pm 1.645 | 0.2928 / 4.656 \pm 1.643 | 0.2528 / 5.092 \pm 1.598 |
| | PCARN | 0.0745 / 4.929 \pm 1.534 | 0.1449 / 5.063 \pm 1.603 | 0.1875 / 5.077 \pm 1.611 | 0.1521 / 5.243 \pm 1.581 |
| | PCARN-M | 0.0796 / 4.865 \pm 1.533 | 0.1502 / 4.981 \pm 1.611 | 0.1981 / 5.010 \pm 1.616 | 0.1671 / 5.180 \pm 1.578 |

- Conference on Signals, Systems & Computers, 2003*, vol. 2. Ieee, 2003, pp. 1398–1402.
- [30] H. R. Sheikh, A. C. Bovik, and G. De Veciana, “An information fidelity criterion for image quality assessment using natural scene statistics,” *IEEE Transactions on image processing*, vol. 14, no. 12, pp. 2117–2128, 2005.
- [31] Y. Blau and T. Michaeli, “The perception-distortion tradeoff,” in *Proceedings of the IEEE Conference on Computer Vision and Pattern Recognition*, 2018, pp. 6228–6237.
- [32] H. Talebi and P. Milanfar, “Nima: Neural image assessment,” *IEEE Transactions on Image Processing*, vol. 27, no. 8, pp. 3998–4011, 2018.
- [33] R. Zhang, P. Isola, A. A. Efros, E. Shechtman, and O. Wang, “The unreasonable effectiveness of deep features as a perceptual metric,” in *CVPR*, 2018.
- [34] J. Deng, W. Dong, R. Socher, L.-J. Li, K. Li, and L. Fei-Fei, “Imagenet: A large-scale hierarchical image database,” in *Proceedings of the Conference on Computer Vision and Pattern Recognition (CVPR)*, 2009.
- [35] A. Krizhevsky, I. Sutskever, and G. E. Hinton, “Imagenet classification with deep convolutional neural networks,” in *Proceedings of the Conference on Neural Information Processing Systems (NIPS)*, 2012.
- [36] A. G. Howard, M. Zhu, B. Chen, D. Kalenichenko, W. Wang, T. Weyand, M. Andreetto, and H. Adam, “Mobilenets: Efficient convolutional neural networks for mobile vision applications,” *arXiv preprint arXiv:1704.04861*, 2017.
- [37] G. Hinton, O. Vinyals, and J. Dean, “Distilling the knowledge in a neural network,” *arXiv preprint arXiv:1503.02531*, 2015.
- [38] A. Romero, N. Ballas, S. E. Kahou, A. Chassang, C. Gatta, and Y. Bengio, “Fitnets: Hints for thin deep nets,” *arXiv preprint arXiv:1412.6550*, 2014.
- [39] L. Sifre and S. Mallat, “Rigid-motion scattering for image classification,” Ph.D. dissertation, Citeseer, 2014.
- [40] F. Chollet, “Xception: Deep learning with depthwise separable convolutions,” in *Proceedings of the Conference on Computer Vision and Pattern Recognition (CVPR)*, 2017.
- [41] X. Zhang, X. Zhou, M. Lin, and J. Sun, “Shufflenet: An extremely efficient convolutional neural network for mobile devices,” in *Proceedings of the Conference on Computer Vision and Pattern Recognition (CVPR)*, 2018.
- [42] N. Ma, X. Zhang, H.-T. Zheng, and J. Sun, “Shufflenet v2: Practical guidelines for efficient cnn architecture design,” in *Proceedings of the European Conference on Computer Vision (ECCV)*, 2018.
- [43] K. He, X. Zhang, S. Ren, and J. Sun, “Deep residual learning for image recognition,” in *Proceedings of the Conference on Computer Vision and Pattern Recognition (CVPR)*, 2016.
- [44] J. Lee and J. Nam, “Multi-level and multi-scale feature aggregation using pretrained convolutional neural networks for music auto-tagging,” *IEEE Signal Processing Letters*, vol. 24, no. 8, pp. 1208–1212, 2017.
- [45] J. Long, E. Shelhamer, and T. Darrell, “Fully convolutional networks for semantic segmentation,” in *Proceedings of the Conference on Computer Vision and Pattern Recognition (CVPR)*, 2015.
- [46] D. Pathak, P. Krahenbuhl, J. Donahue, T. Darrell, and A. A. Efros, “Context encoders: Feature learning by inpainting,” in *Proceedings of the Conference on Computer Vision and Pattern Recognition (CVPR)*, 2016.
- [47] P. Isola, J.-Y. Zhu, T. Zhou, and A. A. Efros, “Image-to-image translation with conditional adversarial networks,” in *Proceedings of the Conference on Computer Vision and Pattern Recognition (CVPR)*, 2017.
- [48] K. Simonyan and A. Zisserman, “Very deep convolutional networks for large-scale image recognition,” *arXiv preprint arXiv:1409.1556*, 2014.
- [49] D. P. Kingma and J. Ba, “Adam: A method for stochastic optimization,” *Proceedings of the International Conference on Learning Representations (ICLR)*, 2015.
- [50] E. Agustsson and R. Timofte, “Ntire 2017 challenge on single image super-resolution: Dataset and study,” in *Proceedings of the Conference on Computer Vision and Pattern Recognition (CVPR) Workshops*, 2017.
- [51] M. Haris, G. Shakhnarovich, and N. Ukita, “Deep backprojection networks for super-resolution,” in *Conference on Computer Vision and Pattern Recognition*, 2018.
- [52] Y. Zhang, Y. Tian, Y. Kong, B. Zhong, and Y. Fu, “Residual dense network for image super-resolution,” in *The IEEE Conference on Computer Vision and Pattern Recognition (CVPR)*, 2018.
- [53] M. Bevilacqua, A. Roumy, C. Guillemot, and M. Alberi-Morel, “Low-complexity single-image super-resolution based on nonnegative neighbor embedding,” in *Proceedings of the British Machine Vision Conference (BMVC)*, 2012.
- [54] J. Yang, J. Wright, T. S. Huang, and Y. Ma, “Image super-resolution via sparse representation,” *IEEE transactions on image processing*, vol. 19, no. 11, pp. 2861–2873, 2010.
- [55] D. Martin, C. Fowlkes, D. Tal, and J. Malik, “A database of human segmented natural images and its application to evaluating segmentation algorithms and measuring ecological statistics,” in *Proceedings of the International Conference on Computer Vision (ICCV)*, 2001.
- [56] J.-B. Huang, A. Singh, and N. Ahuja, “Single image super-resolution from transformed self-exemplars,” in *Proceedings of the Conference on Computer Vision and Pattern Recognition (CVPR)*, 2015.
- [57] K. He, X. Zhang, S. Ren, and J. Sun, “Delving deep into rectifiers: Surpassing human-level performance on imagenet classification,” in *Proceedings of the International Conference on Computer Vision (ICCV)*, 2015.
- [58] H. Ren, M. El-Khamy, and J. Lee, “Image super resolution based on fusing multiple convolution neural networks,” in *Proceedings of the Conference on Computer Vision and Pattern Recognition (CVPR) Workshops*, 2017.
- [59] Y. Fan, H. Shi, J. Yu, D. Liu, W. Han, H. Yu, Z. Wang, X. Wang, and T. S. Huang, “Balanced two-stage residual networks for image super-resolution,” in *Proceedings of the Conference on Computer Vision and Pattern Recognition (CVPR) Workshops*, 2017.
- [60] J.-S. Choi and M. Kim, “A deep convolutional neural network with selection units for super-resolution,” in *Proceedings of the Conference on Computer Vision and Pattern Recognition (CVPR) Workshops*, 2017.
- [61] K. Zhang, W. Zuo, Y. Chen, D. Meng, and L. Zhang, “Beyond a gaussian denoiser: Residual learning of deep cnn for image denoising,” *IEEE Transactions on Image Processing*, vol. 26, no. 7, pp. 3142–3155, 2017.



Namhyuk Ahn Namhyuk Ahn is a Ph.D. candidate of Computer Engineering at Ajou University, South Korea. He received the Bachelor of Media degree from Ajou University in 2016. His research interests include computer vision, image enhancement and efficient deep learning.



Byungkon Kang Byungkon Kang completed his Ph.D. in Computer Science at KAIST in 2013 after receiving his B.S. degree from the University of Texas at Austin in 2006. He had then been employed as a full-time research staff member at Samsung Advanced Institute of Technology until 2016. Since then, Dr. Kang is currently working as a research professor at Ajou University’s Department of Software, specializing in machine learning, natural language processing, and computer vision.



Kyung-Ah Sohn Kyung-Ah Sohn received her Ph.D. in Computer Science from Carnegie Mellon University, USA, in 2011, and M.S and B.S. degrees from Seoul National University, South Korea, in 2003 and 2000, respectively. She was a research professor in the College of Medicine, Seoul National University, in 2012. She is currently an associate professor in the Department of Software and Computer Engineering, Ajou University, South Korea. Her research interest includes statistical machine learning and data mining, computer vision, and biomedical informatics.